AGU PUBLICATIONS

JGR

Journal of Geophysical Research: Space Physics

RESEARCH ARTICLE
10.1002/2015JA021507

Special Section:
Origins and Properties of Kappa Distributions

DSHARK: A dispersion relation solver for obliquely propagating waves in bi-kappa-distributed plasmas

Patrick Astfalk[1], Tobias Görler[1], and Frank Jenko[2]

[1]Max-Planck-Institut für Plasmaphysik, Garching, Germany, [2]Department of Physics and Astronomy, University of California, Los Angeles, California, USA

Abstract Satellite measurements suggest that space plasmas often exhibit bi-kappa particle distributions with high-energy tails instead of simple Maxwellians. The presence of suprathermal particles significantly alters the plasmas' dispersion properties compared to purely Maxwellian scenarios. In the past, wave propagation in magnetized, bi-kappa plasmas was almost exclusively addressed for parallel propagating modes only. To enable a systematic study of both parallel and oblique wave propagation, the new kinetic dispersion relation solver Dispersion Solver for Homogeneous Plasmas with Anisotropic Kappa Distributions (DSHARK) was developed and is presented in this work. DSHARK is an iterative root-finding algorithm which is based on Summers et al. (1994) who derived the dielectric tensor for plasmas with bi-kappa-distributed particles. After a brief discussion of kappa distributions, we present the kinetic theory and the numerical methods implemented in DSHARK and verify the code by considering several test cases. Then, we apply DSHARK to the oblique firehose instability to initiate a more extensive work which will be addressed in the future. A systematic investigation of the dispersion properties of bi-kappa-distributed plasmas is expected to lead to a deeper understanding of wave propagation and instability growth in the solar wind.

Key Points:
- The new dispersion solver DSHARK is presented
- DSHARK determines oblique wave propagation in bi-kappa-distributed plasmas
- DSHARK is applied to the oblique firehose instability

Correspondence to:
P. Astfalk,
patrick.astfalk@ipp.mpg.de

Citation:
Astfalk, P., T. Görler, and F. Jenko (2015), DSHARK: A dispersion relation solver for obliquely propagating waves in bi-kappa-distributed plasmas, *J. Geophys. Res. Space Physics*, *120*, doi:10.1002/2015JA021507.

Received 28 MAY 2015
Accepted 11 AUG 2015
Accepted article online 14 AUG 2015

1. Introduction

Due to the omnipresence of plasmas in the universe, a proper knowledge of the underlying physics is crucial for the correct modeling of many astrophysical systems. A valid description of plasma waves is of major importance here, since the propagation of waves is a ubiquitous property of plasmas and it is connected to the rise of plasma instabilities, particle heating, and turbulence.

The dispersion characteristics of plasma waves crucially depend on the properties of the plasma, such as the presence of background magnetic fields and the shape of the particle velocity distribution function. In sufficiently collisional plasmas, deviations from thermal equilibrium quickly thermalize and the velocity distribution function remains close to a Maxwell-Boltzmann distribution. In this case, wave propagation can often be described by a simple fluid model. However, in dilute space plasmas, which lack collisions, deviations of the velocity distribution from a simple Maxwellian are developed and retained easily. In this case, a kinetic model is favored which often requires a numerical treatment.

In magnetized plasmas, the kinetics of the particles parallel and perpendicular to the background magnetic field decouple, and anisotropic velocity distributions can form which give rise to kinetic instabilities. If the anisotropic distribution follows a bi-Maxwellian,

$$F_\alpha = \frac{1}{\pi^{3/2}} \frac{1}{v_{\parallel\alpha} v_{\perp\alpha}^2} \exp\left(-\frac{v_\parallel^2}{v_{\parallel\alpha}^2} - \frac{v_\perp^2}{v_{\perp\alpha}^2} \right), \tag{1}$$

where $v_\parallel$, $v_\perp$ are the particle velocities parallel and perpendicular to the background magnetic field; m_α is the mass of the particle species α; $v_{\parallel\alpha} = \sqrt{2\frac{T_{\parallel\alpha}}{m_\alpha}}$, $v_{\perp\alpha} = \sqrt{2\frac{T_{\perp\alpha}}{m_\alpha}}$ are the thermal speeds parallel and perpendicular to the magnetic field; and $T_{\alpha\parallel}$, $T_{\alpha\perp}$ denote the associated temperatures; the dispersion properties in the considered medium can be derived numerically by Maxwellian dispersion relation solvers such as WHAMP [*Roennmark*, 1982] or PDRK [*Xie and Xiao*, 2014].

However, real space plasmas are often subject to nonthermal acceleration processes which lead to the formation of non-Maxwellian high-energy velocity tails. These tails rather follow power laws instead of exponentials.

Such suprathermal tails were found for the ion and electron distribution in solar flares [*Achterberg and Norman*, 1980]; in the solar corona [*Ko et al.*, 1996]; in the solar wind [*Gloeckler et al.*, 1992; *Maksimovic et al.*, 1997]; in planetary magnetospheres such as for the Earth [*Paschalidis et al.*, 1994], Jupiter [*Leubner*, 1982], and Saturn [*Krimigis et al.*, 1983]; in the plasma torus of Io [*Meyer-Vernet et al.*, 1995]; farther out in the heliosphere toward the termination shock [*Decker et al.*, 2005], and even in the distribution of galactic cosmic rays [*Jones and Ellison*, 1991]. They can be fitted by so-called kappa distributions which were introduced empirically by *Vasyliunas* [1968] and *Olbert* [1968] to fit electron velocity distributions measured in the Earth's magnetosphere.

Kappa distributions form a group of general power law distributions containing the Maxwell-Boltzmann distribution as a limiting case. Their traditional form is given by

$$F_{\kappa\alpha} = \frac{1}{\pi^{3/2}\kappa^{3/2}} \frac{1}{\theta_{\parallel\alpha}\theta_{\perp\alpha}^2} \frac{\Gamma(\kappa+1)}{\Gamma(\kappa-1/2)} \left(1 + \frac{v_\parallel^2}{\kappa\theta_{\parallel\alpha}^2} + \frac{v_\perp^2}{\kappa\theta_{\perp\alpha}^2}\right)^{-(\kappa+1)}, \tag{2}$$

with the gamma function $\Gamma(x)$ and the modified thermal speeds $\theta_{\parallel\alpha} = \sqrt{\frac{2\kappa-3}{\kappa}\frac{T_{\parallel\alpha}}{m_\alpha}}$ and $\theta_{\perp\alpha} = \sqrt{\frac{2\kappa-3}{\kappa}\frac{T_{\perp\alpha}}{m_\alpha}}$ [*Summers et al.*, 1994]. Observations generally suggest positive kappas with $1.5 < \kappa \leq \infty$. The Maxwellian distribution is recovered in the limit $\kappa \to \infty$.

Note that modified versions of the traditional kappa distribution are also in use, such as the product bi-kappa distribution [*Abraham-Shrauner and Feldman*, 1977; *Summers and Thorne*, 1991]. However, these will not be covered in this paper.

Since their first introduction, kappa distributions have been successfully applied to extensive observational data obtained from space plasma measurements. The vast amount of observational evidence suggests that kappa distributions are not a rare phenomenon but rather omnipresent in space plasmas with low collisionality.

Despite the frequent appearance of suprathermal velocity tails, the mechanisms leading to their formation are still not fully understood. However, there exists a variety of possible explanations, mostly associated with nonlinear wave-particle interaction such as enhanced velocity space diffusion in suprathermal radiation fields [*Hasegawa et al.*, 1985], energization of particles due to nonlinear Landau damping of large-amplitude waves [*Miller*, 1991; *Leubner*, 2000] or stochastic acceleration in compressional turbulence [*Fisk and Gloeckler*, 2006]. Recently, *Yoon* [2012] self-consistently derived the steady state electron distribution function in three-dimensional Langmuir turbulence and found a non-Maxwellian energetic tail component following a kappa-like distribution with $\kappa = 3.25$ which is in rough agreement with measurements of the quiet time solar wind.

A more fundamental approach based on the Tsallis entropy attempts to explain the formation of kappa distributions from basic statistical physics. The applicability of standard Gibbs-Boltzmann statistics to systems which are subject to long-range forces, such as plasmas, has been questioned for a long time. In 1988, Constantino Tsallis proposed a generalization of the Gibbs-Boltzmann entropy which found successful application in a wide range of fields including geology, medicine, meteorology, finance, and plasma physics [*Tsallis*, 1988; *Pavlos et al.*, 2012]. *Silva et al.* [2002] and *Leubner* [2002] showed that Tsallis statistics can be used to derive equilibrium distribution functions which closely resemble the traditional kappa distributions introduced in 1968.

Treumann [1999] constructed a Boltzmann-like collision term accounting for correlations present in a system and derived the corresponding equilibrium distribution function from kinetic theory. Remarkably, this different ansatz yielded the same type of kappa-like distribution as it was obtained from Tsallis statistics by *Leubner* [2002]. This suggests that both kappa distributions and Tsallis entropy are not merely fitting tools but might be indeed the consequence of fundamental physics.

In recent years, it was studied how a change from near-Maxwellian distributions to the more general kappa distributions affects the dispersion properties of wave propagation in space plasmas [see, for example, *Lazar et al.*, 2011; *Leubner and Schupfer*, 2000]. However, as was noticed by *Gaelzer and Ziebell* [2014], the investigations were largely restricted to purely parallel or perpendicular propagation, whereas general oblique propagation has rarely been considered so far. To the authors' knowledge, only *Xue et al.* [1996] properly applied kappa distributions to a case of obliquely propagating modes, namely, ion cyclotron waves in the Earth's magnetosphere.

To enable an extensive and systematic study of the dispersion properties of waves propagating with an arbitrary angle in magnetized plasmas with suprathermal velocity tails, the fast and practical *Dispersion Solver for Homogeneous Plasmas with Anisotropic Kappa Distributions* (DSHARK) was constructed. A description of the physics implemented in DSHARK is provided in section 2. The employed numerical methods are explained in section 3. Section 4 presents some benchmarks and a first application of DSHARK to the oblique firehose instability. A summary is given in section 5.

2. Theoretical Background

For a fully kinetic description of collisionless plasmas, the Vlasov equation is employed which determines the time evolution of the six-dimensional particle distribution function, f ($\mathbf{x}$, $\mathbf{v}$, t). In fluid plasma models, however, the information about the velocity space is removed by assuming a particular velocity distribution — usually a Maxwellian — and deriving the hierarchy of fluid equations by taking the velocity moments of the Vlasov equation. Due to the loss of complexity in the fluid picture, the physics included in a kinetic description is more diverse allowing for a larger variety of possible wave phenomena. Especially waves which undergo resonances with the plasma particles, such as Landau and cyclotron resonance, can only be treated properly within the context of kinetic theory. For the sake of generality, the focus is therefore laid on a fully kinetic plasma description.

From Maxwell's equations, the general dispersion relation for wave propagation in plasmas,

$$0 = \det\left(\frac{c^2k^2}{\omega^2}\left(\frac{\mathbf{k}\otimes\mathbf{k}}{k^2} - \mathbb{1}\right) + \epsilon\right) \tag{3}$$

can be derived, where ϵ is the dielectric tensor of the considered medium and c is the speed of light in vacuum.

The dielectric tensor determines the response of the plasma to small wave-like perturbations and generally depends on the plasma properties. For collisionless plasmas, it can be derived from the linearized Vlasov equation [see, for example, *Brambilla*, 1998].

To enable an analytic treatment, approximations have to be applied which simplify the dielectric tensor components. Some common approximations are the cold plasma limit, pure electrostatics, small Larmor radius approximation, or the restriction to low frequencies. However, to get the full picture, ϵ must be considered in its most general form. This requires a numerical treatment. Thus, for finding the roots, $\omega(\mathbf{k})$, of equation (2) a numerical dispersion relation solver must be applied.

The DSHARK solver, which is presented in this paper, is based on the work done by *Summers et al.* [1994] who derived the dielectric tensor components for a hot, homogeneous, and collisionless plasma which is immersed in a static magnetic field, $\mathbf{B}_0 = B_0\mathbf{e}_z$, and which exhibits high-energy velocity tails following the empirically introduced kappa distribution, equation (2).

For Maxwellian plasmas, the calculation of the dielectric tensor requires the determination of the plasma dispersion function

$$Z(\xi) = \frac{1}{\sqrt{\pi}}\int_{-\infty}^{\infty}\frac{e^{-s^2}}{s-\xi}\,\mathrm{d}s, \tag{4}$$

which was defined by *Fried and Conte* [1961]. The equivalent for kappa-distributed plasmas was found by *Summers and Thorne* [1991] who introduced the corresponding modified dispersion function

$$Z^*_\kappa(\xi) = \frac{1}{\pi^{1/2}\kappa^{3/2}}\frac{\Gamma(\kappa+1)}{\Gamma(\kappa-1/2)}\int_{-\infty}^{\infty}\frac{\mathrm{d}s}{(s-\xi)(1+s^2/\kappa)^{\kappa+1}}. \tag{5}$$

Furthermore, it has been shown in above reference that this can be rewritten in the simple closed form

$$Z^*_\kappa(\xi) = -\frac{\kappa-1/2}{2\kappa^{3/2}}\frac{\kappa!}{(2\kappa)!}\sum_{l=0}^{\kappa}\frac{(\kappa+l)!}{l!}\mathrm{i}^{\kappa-l}\left(\frac{2}{(\xi/\sqrt{\kappa})+\mathrm{i}}\right)^{\kappa+1-l}. \tag{6}$$

Note that the former equation is restricted to the case $\mathrm{Im}(\xi) > 0$, whereas the latter applies for all $\xi \in \mathbb{C}$. One can show that Z^*_κ converges to the standard plasma dispersion function, equation (4), in the limit $\kappa \to \infty$.

Summers et al. [1994] restricted the parameter κ to integer values only. Later, this was generalized by *Mace and Hellberg* [1995] who also discussed noninteger κ.

The presented code solves the dispersion relation, equation (2), using the dielectric tensor given in *Summers et al.* [1994] and allowing for wave propagation with an arbitrary angle θ with respect to the background magnetic field. Furthermore, an arbitrary number of particle species α can be included, where every species is defined by its mass, charge, kappa, and parallel and perpendicular plasma beta. In accordance with *Summers et al.* [1994], the code is restricted to integer κ, only.

The dielectric tensor for bi-Maxwellian plasmas is implemented as well, thus DSHARK can also be used to study dispersion properties in the bi-Maxwellian limit. The expressions for the bi-Maxwellian dielectric tensor used in the code were derived on the basis of *Brambilla* [1998]. For the computation of the corresponding tensor components, the evaluation of the standard plasma dispersion function Z, given in equation (4), is required. A common approximation of Z is the Padé method which was first applied to the plasma dispersion function by *Martin and Gonzalez* [1979] and later used in bi-Maxwellian dispersion solvers such as WHAMP and PDRK. For DSHARK, an eight-pole Padé approximant was used to determine Z. More information on this can be found in Appendix D.

The explicit inclusion of the bi-Maxwellian limit also allows an efficient investigation of hybrid scenarios where one species follows a bi-kappa distribution and another species is Maxwellian.

The dimensionless expressions of the dielectric tensor components used in the code are given in Appendix A and B for both the bi-kappa distribution and the bi-Maxwellian case. The dispersion relation is implemented in the dimensionless form

$$\begin{aligned} 0 = &\left(\hat{\epsilon}_{xx} - \tilde{k}_{\parallel}^2\right)\left(\hat{\epsilon}_{yy} - \tilde{k}^2\right)\left(\hat{\epsilon}_{zz} - \tilde{k}_{\perp}^2\right) + 2\hat{\epsilon}_{xy}\hat{\epsilon}_{yz}\left(\hat{\epsilon}_{xz} + \tilde{k}_{\perp}\tilde{k}_{\parallel}\right) \\ &- \left(\hat{\epsilon}_{yy} - \tilde{k}^2\right)\left(\hat{\epsilon}_{xz} + \tilde{k}_{\perp}\tilde{k}_{\parallel}\right)^2 + \hat{\epsilon}_{yz}^2\left(\hat{\epsilon}_{xz} - \tilde{k}_{\parallel}^2\right) + \hat{\epsilon}_{xy}^2\left(\hat{\epsilon}_{zz} - \tilde{k}_{\perp}^2\right), \end{aligned} \tag{7}$$

with $\hat{\epsilon} = \epsilon\frac{v_A^2}{c^2}\tilde{\omega}^2$ and $\tilde{\omega} = \frac{\omega}{\Omega_i}$ where Ω_i denotes the ion gyro frequency and v_A is the Alfvén velocity, $v_A = B_0/\sqrt{4\pi n_i m_i}$. The wave numbers parallel and perpendicular to the background magnetic field, $\tilde{k}_{\parallel}$ and $\tilde{k}_{\perp}$, are normalized to the ion inertial length, i.e., $\tilde{k} = kd_i$.

If desired, all quantities can be easily normalized to the scales of other involved particle species, instead. However, for the following discussions we keep the given normalization with respect to ions.

3. Numerics

DSHARK is an iterative root-finding algorithm which solves the nonlinear equation (6). Since the frequencies $\tilde{\omega}$ are, in general, expected to be complex valued, the algorithm is required to be able to iterate complex roots. Therefore, Muller's method was implemented which can not only solve complex, nonlinear equations but is also a numerically robust and sufficiently fast procedure (for a description of Muller's method, see, for example, *Gerald and Wheatley* [2003]). As a stopping criterium for the Muller iteration, a limit is set to the relative error of two successively iterated roots, $\epsilon_{rf} = \left|\left(\tilde{\omega}_n - \tilde{\omega}_{n-1}\right)/\tilde{\omega}_{n-1}\right|$. For the test cases presented in section 4, this limit was chosen to be $\epsilon_{rf} = 10^{-3}$. This criterium can be easily adapted by the code user.

The calculation of the tensor components given in Appendix A implies the determination of some improper integrals. For this, an exponential quadrature method was applied. The algorithm implemented in DSHARK was thankfully provided by Takuya Ooura and is based on *Takahasi and Mori* [1974]. The method offers the possibility to set a limit to the relative error of the integral evaluation. This error was chosen to be $\epsilon_{int} = 10^{-12}$ for all calculations carried out in this work.

The integrals to be calculated contain the modified dispersion function $Z_{\kappa+1}^*$ which is determined using the summation formula equation (6). Since the summation in equation (6) goes from $l = 0$ up to $l = \kappa$, the calculation is slowed down if higher kappa values are considered. And since the determination of the integrals containing the modified dispersion function is the most time-consuming task of the algorithm, the chosen kappa value has a crucial influence on the overall performance, reducing the efficiency of the program linearly with kappa. However, for very high kappa values the considered scenario converges to the Maxwellian case. So, if the kappa parameter exceeds a certain default limit, DSHARK automatically switches to a bi-Maxwellian scenario which can be solved more efficiently.

Apart from the chosen kappa values and the considered number of particle species, the performance of DSHARK also crucially depends on the quality of the initial guess of the complex frequency which initiates the iterative Muller method. When the user is not interested in the frequency at a single wave number only, but instead for a whole range of wave numbers, DSHARK automatically applies a quadratic polynomial fit to find proper initial guesses, after the solutions for three subsequent wave numbers are found. This is very effective as long as the interval between subsequent wave numbers is not too large.

For the determination of the dielectric tensor components given in Appendix A, infinite summations over Bessel functions have to be evaluated. Luckily, significant contribution comes from the lowest-order Bessel functions only. Therefore, the sum can normally be restricted to the terms with indices $n = -4, ..., 4$.

More terms might have to be included, if the argument of the Bessel functions becomes too large which is the case, e.g., for high $\tilde{k}_\perp$. However, this can be checked and adapted easily, if necessary.

For a brief overview of the underlying program structure of DSHARK and some further details, see Appendix C.

4. Test Cases

DSHARK determines the dispersion relation for linear waves in hot, collisionless, and homogeneous plasmas. Unlike standard dispersion relation solvers, such as WHAMP, DSHARK is not restricted to plasmas with bi-Maxwellian velocity distributions but it can be used to derive the dispersion relation for plasmas with more general bi-kappa distributions.

Parallel propagating modes in kappa-distributed plasmas have been discussed frequently, whereas oblique propagation has rarely been considered so far. To validate the ability of DSHARK to properly derive the dispersion properties of modes propagating in both parallel and oblique direction, several test cases were considered. A summary of the results is given below.

4.1. Parallel Propagation

Parallel propagating modes in kappa-distributed plasmas have been addressed, e.g., in *Leubner and Schupfer* [2000], *Lazar et al.* [2011], and *Lazar and Poedts* [2014].

By assuming $k_\perp = 0$, a greatly simplified dispersion relation can be constructed from linear kinetic theory. Starting from the well-known general dispersion relation for parallel propagating modes with right-hand (+) and left-hand (−) circular polarization,

$$0 = 1 - \frac{k_\parallel^2 c^2}{\omega^2} + \pi \sum_\alpha \left(\frac{\omega_{p\alpha}}{\omega}\right)^2 \int_{-\infty}^{\infty} dv_\parallel \int_0^{\infty} dv_\perp v_\perp^2 \frac{(\omega - k_\parallel v_\parallel)\frac{\partial f_\alpha}{\partial v_\perp} + k_\parallel v_\perp \frac{\partial f_\alpha}{\partial v_\parallel}}{\omega - k_\parallel v_\parallel \pm \Omega_\alpha}, \tag{8}$$

where $\omega_{p\alpha}$ denotes the plasma frequency of the particle species α [see, for example, *Brambilla*, 1998], one can derive the corresponding model for kappa-distributed plasmas by assuming $f_\alpha = F_{\kappa\alpha}$ and using equation (2).

Following this ansatz, *Lazar et al.* [2011] constructed the dispersion relation

$$0 = 1 - \frac{k_\parallel^2 c^2}{\omega^2} + \sum_\alpha \frac{\omega_{p\alpha}^2}{\omega^2} \left[\frac{\omega}{k_\parallel \theta_{\parallel\alpha}} Z_\kappa^0 \left(\frac{\omega + \Omega_\alpha}{k_\parallel \theta_{\parallel\alpha}}\right) \left(\frac{\beta_{\perp\alpha}}{\beta_{\parallel\alpha}} - 1\right) \left(1 + \frac{\omega + \Omega_\alpha}{k_\parallel \theta_{\parallel\alpha}} Z_\kappa^0 \left(\frac{\omega + \Omega_\alpha}{k_\parallel \theta_{\parallel\alpha}}\right)\right)\right], \tag{9}$$

for right-hand polarized waves by introducing a modified dispersion function Z_k^0. This dispersion function has the form

$$Z_\kappa^0(\xi) = \frac{1}{\sqrt{\pi\kappa}} \frac{\Gamma(\kappa)}{\Gamma(\kappa - 1/2)} \int_{-\infty}^{\infty} \frac{ds}{(s - \xi)\,(1 + s^2/\kappa)^\kappa} \tag{10}$$

and is therefore slightly different but closely related to the standard modified dispersion function Z_κ^*, given by equation (5).

Lazar et al. [2011] investigated the parallel propagating firehose instability in a two-component plasma, consisting of anisotropic electrons and anisotropic ions, for various beta parameters and kappa values. The firehose instability arises in magnetized plasmas where the parallel pressure component sufficiently exceeds the pressure perpendicular to the background magnetic field. Using the ideal MHD equations, a simple dispersion relation can be derived, describing the firehose instability as a fluid instability. However, the dispersion

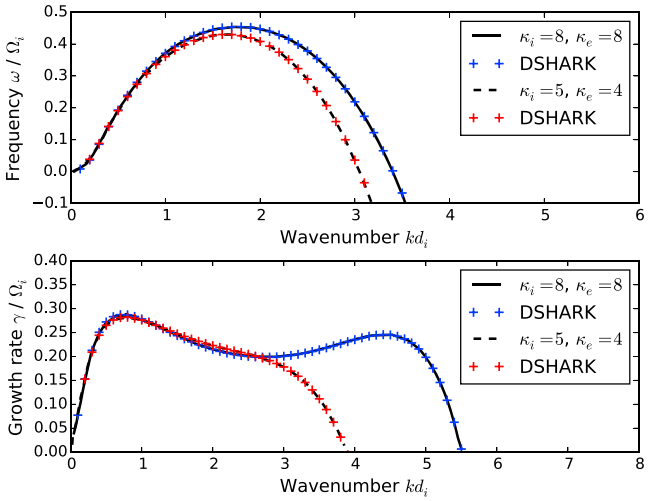

Figure 1. Real frequencies and growth rates of the proton and electron firehose instability derived from equation (9) by *Lazar et al.* [2011] for $\beta_{\|i} = 2.0$, $\beta_{\perp i} = 0.8$, $\beta_{\|e} = 4.0$, $\beta_{\perp e} = 2.0$, and different κ scenarios, compared to the predictions of DSHARK. The solid and dashed curves show the findings of *Lazar et al.* [2011]. The crosses are the corresponding solutions of DSHARK. Blue is for $\kappa_i = 8$, $\kappa_e = 8$, and red is for $\kappa_i = 5$, $\kappa_e = 4$.

properties of the firehose instability are crucially altered by resonance effects. Thus, to capture the whole picture a kinetic model, such as equation (9), has to be used.

Lazar et al. [2011] solved equation (9) to determine the expected growth rates and frequencies for different firehose-unstable setups. To benchmark DSHARK, the same scenarios were tested with the code and it was found that the predictions of DSHARK nicely match the results of *Lazar et al.* [2011]. Two selected cases are shown in Figure 1.

Another case of parallel propagating modes in kappa-distributed plasmas was studied in *Lazar and Poedts* [2014], using the equivalent of equation (9) for left-hand polarized waves. In this work, ion cyclotron modes were investigated which are rendered unstable by an excess of perpendicular pressure and which are also kinetic in nature. Again, good agreement was found between the findings of *Lazar and Poedts* [2014] and the predictions of DSHARK. For illustration, the case of anisotropic ions with $\beta_{\|i}$=1.0, $\beta_{\perp i}$=4.0 and isotropic electrons is shown in Figure 2 for κ_i=2 and the Maxwellian distribution, respectively.

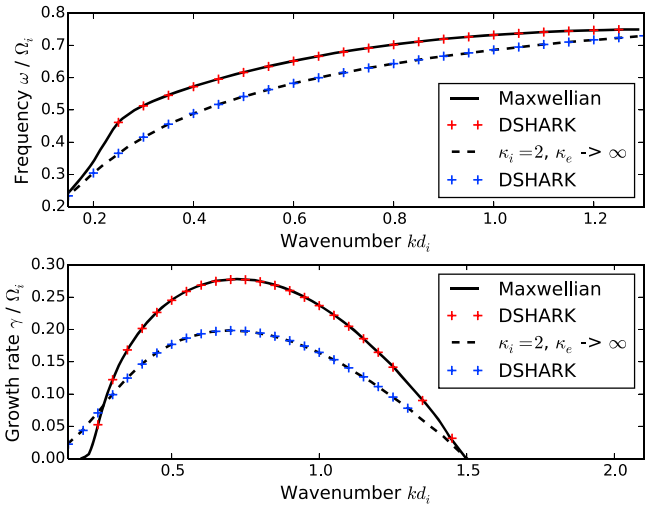

Figure 2. Real frequencies and growth rates of the electromagnetic ion cyclotron instability derived by *Lazar and Poedts* [2014] for $\beta_{\|i} = 1.0$, $\beta_{\perp i} = 4.0$, isotropic Maxwellian electrons, and different κ_i scenarios, compared to the predictions of DSHARK. The solid and dashed curves show the findings of *Lazar and Poedts* [2014]. The crosses are the corresponding solutions of DSHARK. Red is for $\kappa_i = \infty$, $\kappa_e = \infty$, and blue is for $\kappa_i = 2$, $\kappa_e = \infty$.

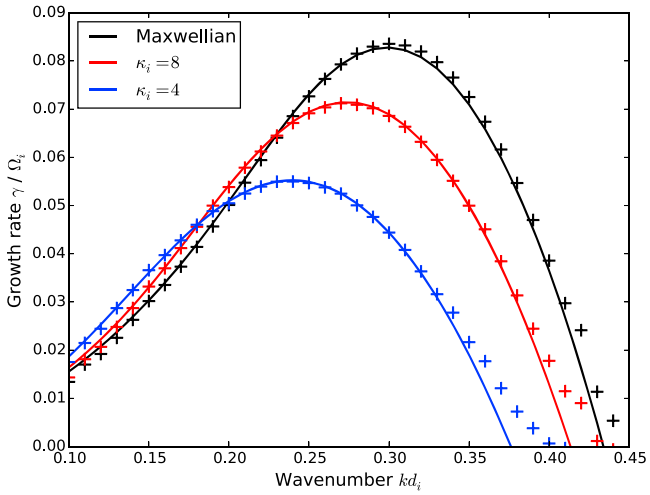

Figure 3. Growth rates observed in HVM simulations of oblique firehose-unstable setups with propagation angle $\theta = 45°$, anisotropic ions with $\beta_{||i} = 4.0$, $\beta_{\perp i} = 1.956$, and isotropic Maxwellian electrons with $\beta_e = \beta_i$ for different κ_i scenarios, compared to the predictions of DSHARK. The solid curves show the observed growth rates. The crosses are the corresponding solutions of DSHARK.

We conclude that DSHARK gives correct predictions for the dispersion properties of parallel propagating modes.

4.2. Oblique Propagation

In kinetic theory, the description of obliquely propagating modes is much more involved than purely parallel propagation since allowing for $k_\perp \neq 0$ gives rise to many additional terms in the general kinetic dispersion relation.

To check the ability of DSHARK to deal with finite propagation angles, numerical simulations of firehose-unstable systems were carried out, using the hybrid Vlasov-Maxwell code (HVM) presented in *Mangeney et al.* [2002] and *Valentini et al.* [2007]. The observed growth rates were then compared to the predictions of DSHARK. In HVM, ions are treated as kinetic particles, whereas electrons are considered as a massless fluid.

As a first test case of oblique propagation, a magnetized plasma with an initially anisotropic bi-Maxwellian ion distribution function was simulated where the ion plasma betas were set to $\beta_{||i} = 4.0$ and $\beta_{\perp i} = 1.956$, and the electrons were assumed to be isotropic with $\beta_e = 2.637$. Due to the initial excess of parallel ion pressure the oblique firehose instability is driven in this scenario. The oblique firehose instability is kinetic in nature and purely growing [*Hellinger and Matsumoto*, 2000].

The simulation setup was chosen to be one-dimensional in position and three-dimensional in velocity space, and the spatial grid was tilted with respect to the background magnetic field by $\theta = 45°$. The oblique firehose instability was excited by random noise perturbations in the initial magnetic field amplitudes.

The observed growth rates for the unstable modes were obtained from spectral analysis and are shown as crosses in Figure (3, black). As can be seen in Figure 3 (black), good agreement was found between the growth rates observed in the HVM simulation and the predictions by DSHARK.

As a next step, the same setup was also tested for two low-kappa scenarios. Instead of a bi-Maxwellian, HVM was initiated with ion bi-kappa distributions with $\kappa_i = 4$ and $\kappa_i = 8$, respectively. Again, good agreement was found between the observed growth rates and the predictions of DSHARK (see Figure 3, red and blue).

The slight offset between the curves at higher wave number k is supposed to stem from the fact that the HVM code was used in the Hall-MHD limit. Since the electrons are treated as a fluid in this approximation, deviations from the fully kinetic case might arise at small length scales. However, this will be subject of future investigations.

We conclude that DSHARK properly solves the general dispersion relation also for waves with finite propagation angles $\theta \neq 0°$.

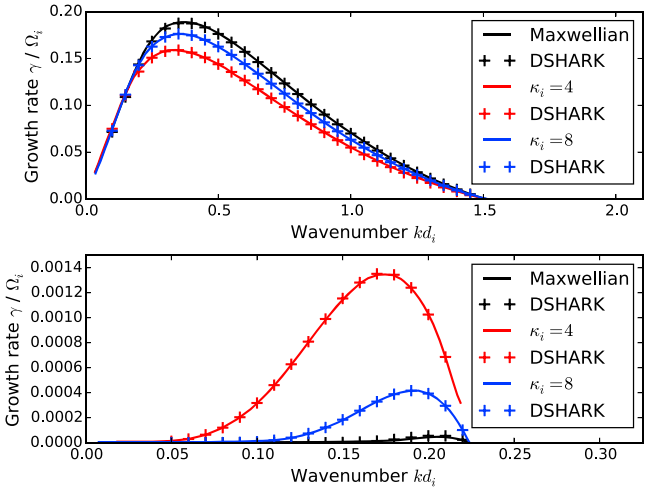

Figure 4. Growth rates of the parallel firehose instability derived from equation (9) by *Lazar et al.* [2011] for anisotropic ions with $\beta_{\|i} = 4.0$ and (top) high anisotropy $\beta_{\perp i}/\beta_{\|i} = 0.25$ and (bottom) low anisotropy $\beta_{\perp i}/\beta_{\|i} = 0.8$ for different κ_i scenarios, compared to the predictions of DSHARK. The electrons are isotropic and Maxwellian with $\beta_e = 8$. The solid curves show the findings of *Lazar et al.* [2011]. The crosses are the corresponding solutions of DSHARK.

4.3. The Oblique Firehose Instability in Bi-kappa Plasmas

To the authors' knowledge, the effect of suprathermal particles on the dispersion properties of the oblique firehose instability has not been considered so far. Therefore, a more detailed investigation was started.

Lazar et al. [2011] and *Lazar and Poedts* [2014] studied how the presence of suprathermal particles changes the growth rate of the parallel firehose instability and the growth rate of the electromagnetic ion cyclotron instability. In both cases, it was discovered that for high anisotropies the growth is enhanced with increasing kappa, reaching a maximum for the Maxwellian case, $\kappa \to \infty$, while for low anisotropies increasing growth rates were observed for decreasing kappa. This is illustrated in Figure 4 for a parallel firehose setup which was investigated in *Lazar et al.* [2011] and in Figure 5 for an ion cyclotron-unstable setup which was investigated in *Lazar and Poedts* [2014]. Both scenarios were successfully recovered by DSHARK.

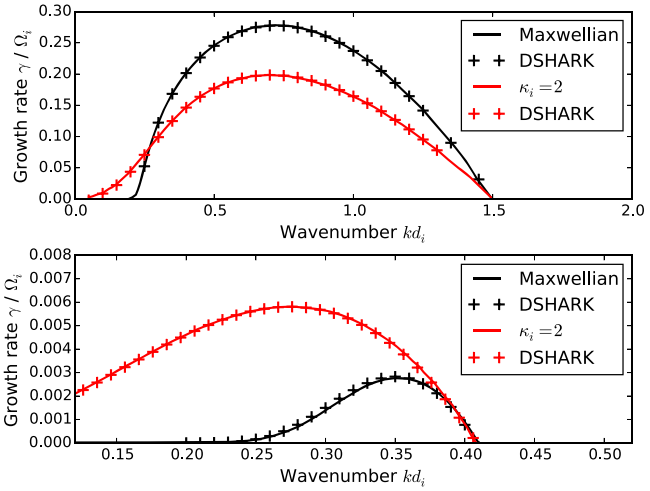

Figure 5. Growth rates of the electromagnetic ion cyclotron instability derived by *Lazar and Poedts* [2014] for anisotropic ions with $\beta_{\|i} = 1.0$ and (top) high anisotropy $\beta_{\perp i}/\beta_{\|i} = 4.0$ and (bottom) low anisotropy $\beta_{\perp i}/\beta_{\|i} = 1.5$ for different κ_i scenarios, compared to the predictions of DSHARK. The electrons are isotropic and Maxwellian. The solid curves show the findings of *Lazar and Poedts* [2014]. The crosses are the corresponding solutions of DSHARK.

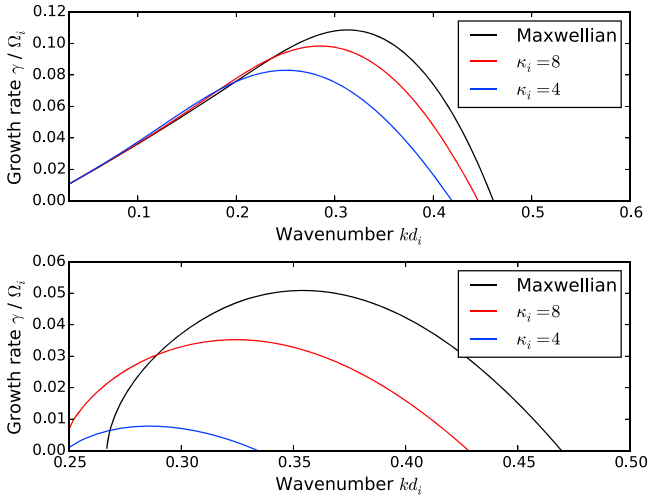

Figure 6. Growth rates of firehose-unstable modes with propagation angle $\theta = 45°$ predicted by DSHARK for different κ_i setups with anisotropic ions with $\beta_{||i} = 3.0$ and (top) high anisotropy $\beta_{||i}/\beta_{\perp i} = 6$ and (bottom) low anisotropy $\beta_{||i}/\beta_{\perp i} = 2.2$. The electrons are isotropic and Maxwellian with $\beta_e = \beta_i$.

First, investigations of the oblique firehose instability suggest a different behavior. For firehose-unstable modes with propagation angle $\theta = 45°$, the Maxwellian scenario always dominates over low-kappa setups for both, high and low anisotropies. This is shown in Figure 6 for a low-beta scenario. In oblique firehose-unstable setups, the presence of suprathermal particles always seems to lead to a reduction of the maximum growth rate. This suggests that a decrease of kappa raises the instability threshold to higher-temperature anisotropies. However, a systematic and extensive analysis of this will be presented in a separate paper.

5. Summary

Satellite measurements in the solar wind suggest that particle velocity distributions in collisionless plasmas tend to develop suprathermal tails. The resulting distributions exhibit power law slopes which can be fitted by so-called kappa distributions [*Vasyliunas*, 1968; *Olbert*, 1968]. The presence of suprathermal particles can significantly change the dispersion properties of plasma waves with respect to the Maxwellian case. In the past, this was studied for wave vectors which are aligned with the background magnetic field, while the general case of obliquely propagating modes was rarely addressed.

In this paper, the newly developed dispersion relation solver DSHARK was presented which is based on *Summers et al.* [1994] and which allows the systematic investigation of wave propagation with arbitrary propagation angle in the presence of an arbitrary number of bi-kappa-distributed particle species. The underlying physics and algorithms were discussed and several test cases were presented. In comparison with former work [*Lazar et al.*, 2011; *Lazar and Poedts*, 2014] and with hybrid simulations it was shown that DSHARK properly derives the correct dispersion relations for both parallel and obliquely propagating modes.

After this successful validation, DSHARK can now be applied to systematically study how the presence of high-energy particles changes, e.g., the growth rates and instability thresholds of kinetic instabilities with $k_{||}, k_{\perp} \neq 0$ such as the oblique firehose or the mirror instability. Such investigations will be addressed in an upcoming paper and might lead to a better understanding of the pressure anisotropies observed in the solar wind.

Appendix A: Dimensionless Components of the Dielectric Tensor for Bi-kappa Plasmas

Summers et al. [1994] derived the dielectric tensor for a hot collisionless plasma which is immersed in a static background magnetic field $\mathbf{B}_0 = B_0\mathbf{e}_z$ and which contains suprathermal particles following a kappa distribution of the form given in equation (2). Introducing the dimensionless quantities $\tilde{\omega} = \omega/\Omega_i$, $\tilde{k} = kd_i$, $\mu_\alpha = m_i/m_\alpha$ and $\tilde{q}_\alpha = q_\alpha/q_i$, the tensor components can be written in the form given below, where $J_n(x)$ and $J_n'(x)$ denote the Bessel function of the first kind and its derivative.

The diagonal elements of the dielectric tensor are then given by

$$\epsilon_{xx} = 1 + \sum_\alpha \frac{c^2}{v_A^2}\frac{1}{\tilde{\omega}^2}\mu_\alpha \tilde{q}_\alpha^2 \left(\frac{\beta_{\perp\alpha}}{\beta_{\parallel\alpha}} - 1\right) + \sum_\alpha \frac{c^2}{v_A^2}\frac{4\sqrt{2}}{\tilde{\omega}^2}\mu_\alpha^{3/2}\tilde{q}_\alpha^4 \frac{\kappa_\alpha - 1/2}{\beta_{\perp\alpha}\tilde{k}_\perp^2\sqrt{\beta_{\parallel\alpha}}\tilde{k}_\parallel}\left(\frac{\kappa_\alpha + 1}{2\kappa_\alpha - 3}\right)^{3/2}\sum_{n=-\infty}^{\infty} n^2$$
$$\times\left(\frac{\beta_{\perp\alpha}}{\beta_{\parallel\alpha}}\omega - n\mu_\alpha\tilde{q}_\alpha\left(\frac{\beta_{\perp\alpha}}{\beta_{\parallel\alpha}} - 1\right)\right)\int_1^\infty \mathrm{d}s\, \frac{J_n^2\left(\frac{\tilde{k}_\perp}{\tilde{q}_\alpha}\sqrt{\frac{(2\kappa_\alpha-3)\beta_{\perp\alpha}}{2\mu_\alpha}(s-1)}\right)}{s^{\kappa_\alpha+2}} Z_{\kappa+1}^*\left(\sqrt{\frac{2\kappa_\alpha+2}{2\kappa_\alpha-3}}\frac{\tilde{\omega} - n\tilde{q}_\alpha\mu_\alpha}{\tilde{k}_\parallel\sqrt{\beta_{\parallel\alpha}\mu_\alpha s}}\right),$$

$$\epsilon_{yy} = 1 + \sum_\alpha \frac{c^2}{v_A^2}\frac{1}{\tilde{\omega}^2}\mu_\alpha \tilde{q}_\alpha^2 \left(\frac{\beta_{\perp\alpha}}{\beta_{\parallel\alpha}} - 1\right) + \sum_\alpha \frac{c^2}{v_A^2}\frac{2\sqrt{2}}{\tilde{\omega}^2}\sqrt{\mu_\alpha}\tilde{q}_\alpha^2 \frac{\kappa_\alpha - 1/2}{\sqrt{\beta_{\parallel\alpha}}\tilde{k}_\parallel}\frac{(\kappa_\alpha+1)^{3/2}}{\sqrt{2\kappa_\alpha-3}}\sum_{n=-\infty}^{\infty}\left(\frac{\beta_{\perp\alpha}}{\beta_{\parallel\alpha}}\omega\right.$$
$$\left. - n\mu_\alpha\tilde{q}_\alpha\left(\frac{\beta_{\perp\alpha}}{\beta_{\parallel\alpha}} - 1\right)\right)\int_1^\infty \mathrm{d}s\,(s-1)\frac{J_n'^2\left(\frac{\tilde{k}_\perp}{\tilde{q}_\alpha}\sqrt{\frac{(2\kappa_\alpha-3)\beta_{\perp\alpha}}{2\mu_\alpha}(s-1)}\right)}{s^{\kappa_\alpha+2}} Z_{\kappa+1}^*\left(\sqrt{\frac{2\kappa_\alpha+2}{2\kappa_\alpha-3}}\frac{\tilde{\omega} - n\tilde{q}_\alpha\mu_\alpha}{\tilde{k}_\parallel\sqrt{\beta_{\parallel\alpha}\mu_\alpha s}}\right),$$

$$\epsilon_{zz} = 1 + \sum_\alpha \frac{c^2}{v_A^2}\frac{1}{\tilde{\omega}^2}\mu_\alpha \tilde{q}_\alpha^2 \left(\frac{\beta_{\perp\alpha}}{\beta_{\parallel\alpha}} - 1\right)\frac{\tilde{k}_\perp^2}{\tilde{k}_\parallel^2} + \sum_\alpha \frac{c^2}{v_A^2}\tilde{q}_\alpha^2\frac{2}{\beta_{\parallel\alpha}\tilde{k}_\parallel^2}\frac{2\kappa_\alpha - 1}{2\kappa_\alpha - 3} + \sum_\alpha \frac{c^2}{v_A^2}\frac{4\sqrt{2}}{\tilde{\omega}^2}\frac{\tilde{q}_\alpha^2}{\sqrt{\mu_\alpha}}\frac{\kappa_\alpha - 1/2}{\beta_{\perp\alpha}\sqrt{\beta_{\parallel\alpha}}\tilde{k}_\parallel^3}$$
$$\times\left(\frac{\kappa_\alpha+1}{2\kappa_\alpha-3}\right)^{3/2}\sum_{n=-\infty}^{\infty}\left(\frac{\beta_{\perp\alpha}}{\beta_{\parallel\alpha}}\omega - n\mu_\alpha\tilde{q}_\alpha\left(\frac{\beta_{\perp\alpha}}{\beta_{\parallel\alpha}} - 1\right)\right)(\omega - n\mu_\alpha\tilde{q}_\alpha)^2$$
$$\times\int_1^\infty \mathrm{d}s\, \frac{J_n^2\left(\frac{\tilde{k}_\perp}{\tilde{q}_\alpha}\sqrt{\frac{(2\kappa_\alpha-3)\beta_{\perp\alpha}}{2\mu_\alpha}(s-1)}\right)}{s^{\kappa_\alpha+2}} Z_{\kappa+1}^*\left(\sqrt{\frac{2\kappa_\alpha+2}{2\kappa_\alpha-3}}\frac{\tilde{\omega} - n\tilde{q}_\alpha\mu_\alpha}{\tilde{k}_\parallel\sqrt{\beta_{\parallel\alpha}\mu_\alpha s}}\right).$$

The off-diagonal elements can be expressed as

$$\epsilon_{xy} = \mathrm{i}\sum_\alpha \frac{c^2}{v_A^2}\frac{4}{\tilde{\omega}^2}\mu_\alpha\tilde{q}_\alpha^3\frac{\kappa_\alpha - 1/2}{\sqrt{\beta_{\perp\alpha}}\tilde{k}_\perp\sqrt{\beta_{\parallel\alpha}}\tilde{k}_\parallel}\frac{(\kappa_\alpha+1)^{3/2}}{2\kappa_\alpha-3}\sum_{n=-\infty}^{\infty} n\left(\frac{\beta_{\perp\alpha}}{\beta_{\parallel\alpha}}\omega - n\mu_\alpha\tilde{q}_\alpha\left(\frac{\beta_{\perp\alpha}}{\beta_{\parallel\alpha}} - 1\right)\right)$$
$$\times\int_1^\infty \mathrm{d}s\,\sqrt{s-1}\frac{J_n\left(\frac{\tilde{k}_\perp}{\tilde{q}_\alpha}\sqrt{\frac{(2\kappa_\alpha-3)\beta_{\perp\alpha}}{2\mu_\alpha}(s-1)}\right)J_n'\left(\frac{\tilde{k}_\perp}{\tilde{q}_\alpha}\sqrt{\frac{(2\kappa_\alpha-3)\beta_{\perp\alpha}}{2\mu_\alpha}(s-1)}\right)}{s^{\kappa_\alpha+2}} Z_{\kappa+1}^*\left(\sqrt{\frac{2\kappa_\alpha+2}{2\kappa_\alpha-3}}\frac{\tilde{\omega} - n\tilde{q}_\alpha\mu_\alpha}{\tilde{k}_\parallel\sqrt{\beta_{\parallel\alpha}\mu_\alpha s}}\right),$$

$$\epsilon_{xz} = -\sum_\alpha \frac{c^2}{v_A^2}\frac{1}{\tilde{\omega}^2}\mu_\alpha\tilde{q}_\alpha^2\left(\frac{\beta_{\perp\alpha}}{\beta_{\parallel\alpha}} - 1.0\right)\frac{\tilde{k}_\perp^2}{\tilde{k}_\parallel^2} + \sum_\alpha \frac{c^2}{v_A^2}\frac{4\sqrt{2}}{\tilde{\omega}^2}\sqrt{\mu_\alpha}\tilde{q}_\alpha^3\frac{\kappa_\alpha - 1/2}{\beta_{\perp\alpha}\tilde{k}_\perp\sqrt{\beta_{\parallel\alpha}}\tilde{k}_\parallel^2}\left(\frac{\kappa_\alpha+1}{2\kappa_\alpha-3}\right)^{3/2}\sum_{n=-\infty}^{\infty} n\left(\frac{\beta_{\perp\alpha}}{\beta_{\parallel\alpha}}\omega\right.$$
$$\left. - n\mu_\alpha\tilde{q}_\alpha\left(\frac{\beta_{\perp\alpha}}{\beta_{\parallel\alpha}} - 1\right)\right)(\omega - n\mu_\alpha\tilde{q}_\alpha)\int_1^\infty \mathrm{d}s\, \frac{J_n^2\left(\frac{\tilde{k}_\perp}{\tilde{q}_\alpha}\sqrt{\frac{(2\kappa_\alpha-3)\beta_{\perp\alpha}}{2\mu_\alpha}(s-1)}\right)}{s^{\kappa_\alpha+2}} Z_{\kappa+1}^*\left(\sqrt{\frac{2\kappa_\alpha+2}{2\kappa_\alpha-3}}\frac{\tilde{\omega} - n\tilde{q}_\alpha\mu_\alpha}{\tilde{k}_\parallel\sqrt{\beta_{\parallel\alpha}\mu_\alpha s}}\right),$$

$$\epsilon_{yz} = -\mathrm{i}\sum_\alpha \frac{c^2}{v_A^2}\frac{4}{\tilde{\omega}^2}\tilde{q}_\alpha^2\frac{\kappa_\alpha - 1/2}{\sqrt{\beta_{\perp\alpha}}\sqrt{\beta_{\parallel\alpha}}\tilde{k}_\parallel^2}\frac{(\kappa_\alpha+1)^{3/2}}{2\kappa_\alpha-3}\sum_{n=-\infty}^{\infty}\left(\frac{\beta_{\perp\alpha}}{\beta_{\parallel\alpha}}\omega - n\mu_\alpha\tilde{q}_\alpha\left(\frac{\beta_{\perp\alpha}}{\beta_{\parallel\alpha}} - 1\right)\right)(\omega - n\mu_\alpha\tilde{q}_\alpha)$$
$$\times\int_1^\infty \mathrm{d}s\,\sqrt{s-1}\frac{J_n\left(\frac{\tilde{k}_\perp}{\tilde{q}_\alpha}\sqrt{\frac{(2\kappa_\alpha-3)\beta_{\perp\alpha}}{2\mu_\alpha}(s-1)}\right)J_n'\left(\frac{\tilde{k}_\perp}{\tilde{q}_\alpha}\sqrt{\frac{(2\kappa_\alpha-3)\beta_{\perp\alpha}}{2\mu_\alpha}(s-1)}\right)}{s^{\kappa_\alpha+2}} Z_{\kappa+1}^*\left(\sqrt{\frac{2\kappa_\alpha+2}{2\kappa_\alpha-3}}\frac{\tilde{\omega} - n\tilde{q}_\alpha\mu_\alpha}{\tilde{k}_\parallel\sqrt{\beta_{\parallel\alpha}\mu_\alpha s}}\right),$$

and one can find the useful symmetry relations $\epsilon_{yx} = -\epsilon_{xy}$, $\epsilon_{zx} = \epsilon_{xz}$, and $\epsilon_{zy} = -\epsilon_{yz}$.

Appendix B: Dimensionless Components of the Dielectric Tensor for Bi-Maxwellian Plasmas

On the basis of *Brambilla* [1998], the dielectric tensor was derived for a hot collisionless plasma which is subject to a static background magnetic field $\mathbf{B}_0 = B_0\mathbf{e}_z$ and which exhibits a bi-Maxwellian particle velocity distribution function of the form given in equation (1). The same normalizations are used as in Appendix A.

$I_n(x)$ and $I_n'(x)$ denote the modified Bessel function of the first kind and its derivative, and the abbreviation $\lambda_\alpha = \frac{\beta_{\perp\alpha}\tilde{k}_\perp^2}{2\mu_\alpha\tilde{q}_\alpha^2}$ is used.

The diagonal elements of the bi-Maxwellian dielectric tensor are then given by

$$\begin{aligned}
\epsilon_{xx} =& 1 + \sum_\alpha \frac{c^2}{v_A^2}\frac{1}{\tilde{\omega}^2}\mu_\alpha\tilde{q}_\alpha^2\left(\frac{\beta_{\perp\alpha}}{\beta_{\parallel\alpha}} - 1\right) + \sum_\alpha \frac{c^2}{v_A^2}\frac{1}{\tilde{\omega}^2}\sqrt{\mu_\alpha}\tilde{q}_\alpha^2\frac{1}{\sqrt{\beta_{\parallel\alpha}}\tilde{k}_\parallel}\sum_{n=-\infty}^{\infty} n^2 I_n\left(\lambda_\alpha\right) \\
&\times \frac{e^{-\lambda_\alpha}}{\lambda_\alpha}\left(\frac{\beta_{\perp\alpha}}{\beta_{\parallel\alpha}}\tilde{\omega} - \left(\frac{\beta_{\perp\alpha}}{\beta_{\parallel\alpha}} - 1\right)n\mu_\alpha\tilde{q}_\alpha\right) Z\left(\frac{\tilde{\omega} - n\mu_\alpha\tilde{q}_\alpha}{\sqrt{\mu_\alpha}\sqrt{\beta_{\parallel\alpha}}\tilde{k}_\parallel}\right), \\
\epsilon_{yy} =& 1 + \sum_\alpha \frac{c^2}{v_A^2}\frac{1}{\tilde{\omega}^2}\mu_\alpha\tilde{q}_\alpha^2\left(\frac{\beta_{\perp\alpha}}{\beta_{\parallel\alpha}} - 1\right) + \sum_\alpha \frac{c^2}{v_A^2}\frac{1}{\tilde{\omega}^2}\sqrt{\mu_\alpha}\tilde{q}_\alpha^2\frac{1}{\sqrt{\beta_{\parallel\alpha}}\tilde{k}_\parallel}\sum_{n=-\infty}^{\infty}\left(n^2\frac{I_n\left(\lambda_\alpha\right)}{\lambda_\alpha}\right. \\
&\left. -2\lambda_\alpha\left(I_n'\left(\lambda_\alpha\right) - I_n\left(\lambda_\alpha\right)\right)\right) e^{-\lambda_\alpha}\left(\frac{\beta_{\perp\alpha}}{\beta_{\parallel\alpha}}\tilde{\omega} - \left(\frac{\beta_{\perp\alpha}}{\beta_{\parallel\alpha}} - 1\right)n\mu_\alpha\tilde{q}_\alpha\right) Z\left(\frac{\tilde{\omega} - n\mu_\alpha\tilde{q}_\alpha}{\sqrt{\mu_\alpha}\sqrt{\beta_{\parallel\alpha}}\tilde{k}_\parallel}\right), \\
\epsilon_{zz} =& 1 - \sum_\alpha \frac{c^2}{v_A^2}\frac{1}{\tilde{\omega}^2}\tilde{q}_\alpha^2\frac{1}{\beta_{\perp\alpha}\tilde{k}_\parallel^2}\sum_{n=-\infty}^{\infty} I_n\left(\lambda_\alpha\right) e^{-\lambda_\alpha}\left(\frac{\beta_{\perp\alpha}}{\beta_{\parallel\alpha}}\tilde{\omega} - \left(\frac{\beta_{\perp\alpha}}{\beta_{\parallel\alpha}} - 1\right)n\mu_\alpha\tilde{q}_\alpha\right) \\
&\times\left(\tilde{\omega} - n\mu_\alpha\tilde{q}_\alpha\right) Z'\left(\frac{\tilde{\omega} - n\mu_\alpha\tilde{q}_\alpha}{\sqrt{\mu_\alpha}\sqrt{\beta_{\parallel\alpha}}\tilde{k}_\parallel}\right).
\end{aligned}$$

The off-diagonal elements can be expressed as

$$\begin{aligned}
\epsilon_{xy} =& \mathrm{i}\sum_\alpha \frac{c^2}{v_A^2}\frac{1}{\tilde{\omega}^2}\mu_\alpha\tilde{q}_\alpha^2\sum_{n=-\infty}^{\infty} n\left(I_n'\left(\lambda_\alpha\right) - I_n\left(\lambda_\alpha\right)\right) e^{-\lambda_\alpha}\left(\frac{\beta_{\perp\alpha}}{\beta_{\parallel\alpha}} - 1\right) + \mathrm{i}\sum_\alpha \frac{c^2}{v_A^2}\frac{1}{\tilde{\omega}^2}\sqrt{\mu_\alpha}\tilde{q}_\alpha^2\frac{1}{\sqrt{\beta_{\parallel\alpha}}\tilde{k}_\parallel} e^{-\lambda_\alpha} \\
&\times\sum_{n=-\infty}^{\infty} n\left(I_n'\left(\lambda_\alpha\right) - I_n\left(\lambda_\alpha\right)\right)\left(\frac{\beta_{\perp\alpha}}{\beta_{\parallel\alpha}}\tilde{\omega} - \left(\frac{\beta_{\perp\alpha}}{\beta_{\parallel\alpha}} - 1\right)n\mu_\alpha\tilde{q}_\alpha\right) Z\left(\frac{\tilde{\omega} - n\mu_\alpha\tilde{q}_\alpha}{\sqrt{\mu_\alpha}\sqrt{\beta_{\parallel\alpha}}\tilde{k}_\parallel}\right) \\
\epsilon_{xz} =& -\sum_\alpha \frac{c^2}{v_A^2}\frac{1}{\tilde{\omega}^2}\mu_\alpha\tilde{q}_\alpha^3\frac{1}{\beta_{\perp\alpha}\tilde{k}_\perp}\frac{1}{\tilde{k}_\parallel}\sum_{n=-\infty}^{\infty} n I_n\left(\lambda_\alpha\right) e^{-\lambda_\alpha}\left(\frac{\beta_{\perp\alpha}}{\beta_{\parallel\alpha}}\tilde{\omega} - \left(\frac{\beta_{\perp\alpha}}{\beta_{\parallel\alpha}} - 1\right)n\mu_\alpha\tilde{q}_\alpha\right) Z'\left(\frac{\tilde{\omega} - n\mu_\alpha\tilde{q}_\alpha}{\sqrt{\mu_\alpha}\sqrt{\beta_{\parallel\alpha}}\tilde{k}_\parallel}\right) \\
\epsilon_{yz} =& \frac{\mathrm{i}}{2}\sum_\alpha \frac{c^2}{v_A^2}\frac{1}{\tilde{\omega}^2}\tilde{q}_\alpha\frac{\tilde{k}_\perp}{\tilde{k}_\parallel}\sum_{n=-\infty}^{\infty}\left(I_n'\left(\lambda_\alpha\right) - I_n\left(\lambda_\alpha\right)\right) e^{-\lambda_\alpha}\left(\frac{\beta_{\perp\alpha}}{\beta_{\parallel\alpha}}\tilde{\omega} - \left(\frac{\beta_{\perp\alpha}}{\beta_{\parallel\alpha}} - 1\right)n\mu_\alpha\tilde{q}_\alpha\right) Z'\left(\frac{\tilde{\omega} - n\mu_\alpha\tilde{q}_\alpha}{\sqrt{\mu_\alpha}\sqrt{\beta_{\parallel\alpha}}\tilde{k}_\parallel}\right)
\end{aligned}$$

and one finds the same symmetry relations as in Appendix A, namely, $\epsilon_{yx} = -\epsilon_{xy}$, $\epsilon_{zx} = \epsilon_{xz}$, and $\epsilon_{zy} = -\epsilon_{yz}$.

Appendix C: Algorithm of DSHARK

This section is intended to give a brief overview of the underlying program structure of the Fortran 90 code DSHARK which is schematically shown in Figure C1.

The core of DSHARK is an iterative root-finding algorithm enclosed by a loop over the considered wave number interval. Before the loop is started, all necessary parameters are read from an input file by the routine *read_data*(). The input provides the iterative root-finding algorithm with the initial guesses ω_{ini} for the first three wave numbers $\mathbf{k}_i$, $i = 0, 1, 2$. For all subsequent wave numbers, the initial guesses are determined by the routine *polyfit*() which uses quadratic polynomials to fit the previous solutions.

Starting from the supplied initial guess and the given wave number $\mathbf{k}$, the routine *muller*() iterates a complex root $\omega(\mathbf{k})$ of equation (2) using the Muller method. Thus, for every iteration the right-hand side of equation (2) has to be evaluated which requires the determination of the dielectric tensor components. This is done by the routine *disp_det*(). All necessary integrations are carried out with the subroutine *integrator*() which uses a

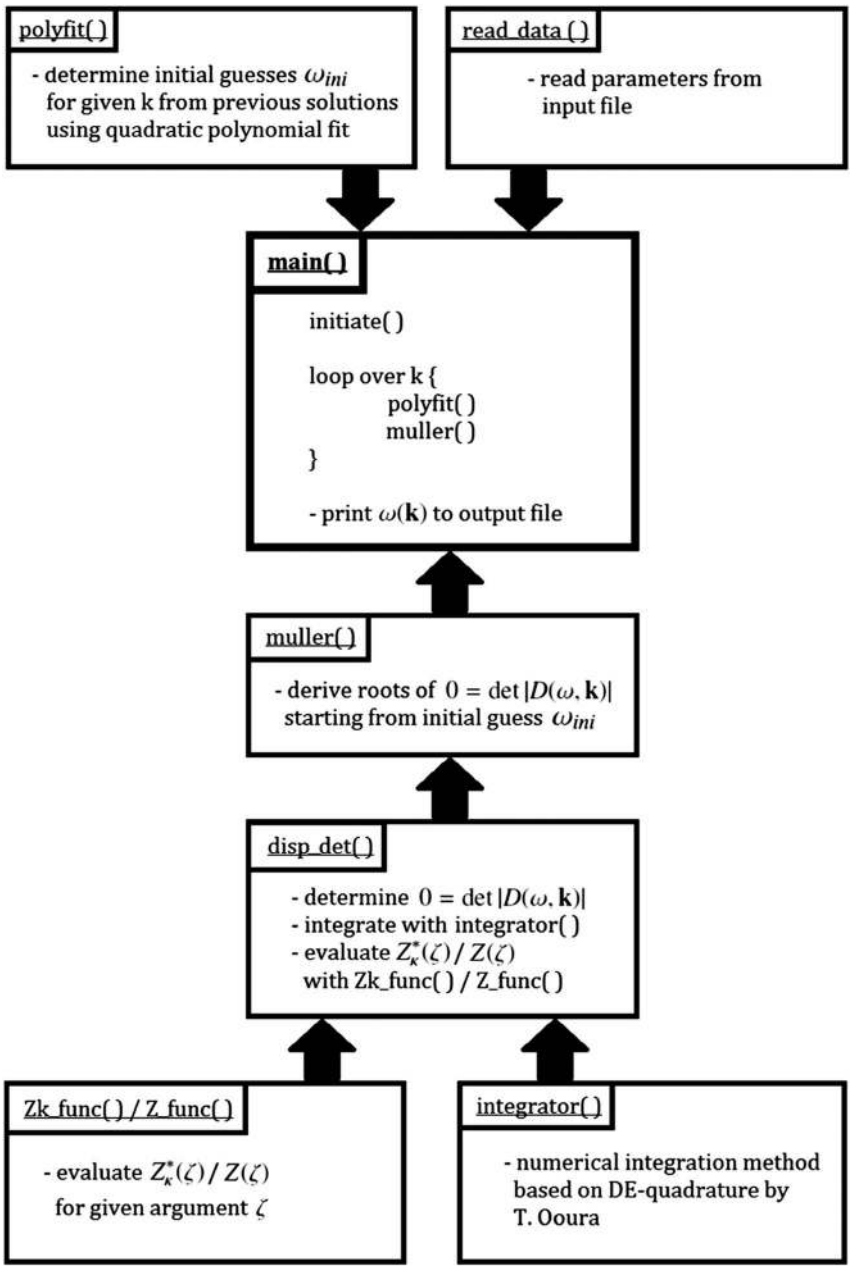

Figure C1. Sketch of the program structure of DSHARK.

double exponential quadrature method provided by Takuya Ooura. The evaluation of the plasma dispersion function and the modified plasma dispersion function is done by separate functions *Z_func*() and *Zk_func*().

After the loop successfully cycles through the wave number interval, all roots are printed to an output file.

Appendix D: Padé Approximation of the Plasma Dispersion Function

The standard plasma dispersion function Z defined by *Fried and Conte* [1961] can be approximated using a modified Padé method [*Martin and Gonzalez*, 1979]. In accordance to other dispersion solvers such as WHAMP and PDRK, DSHARK adopted an eight-pole approximant,

$$Z(\xi) \approx \sum_{j=1}^{8} \frac{b_j}{\xi - c_j}, \tag{D1}$$

with complex coefficients b_j, c_j, given in Table D1.

Table D1. Coefficients of the Eight-Pole Padé Approximation for the Plasma Dispersion Function Z, Given in Equation (D1)[a]

j	b_j	c_j
1	−0.017340124574718 − 0.04630639291680i	2.237687789201900 − 1.625940856173727i
2	−0.739916992322501 + 0.83951799780998i	1.465234126106004 − 1.789620129162444i
3	5.840628642184073 + 0.95360090576437i	0.839253981723264 − 1.891995045765206i
4	−5.583371525286853 − 11.20854319126599i	0.273936222628556 − 1.941786875844713i
	$b_{5,6,7,8} = b^*_{1,2,3,4}$	$c_{5,6,7,8} = -c^*_{1,2,3,4}$

[a]The coefficients were taken from *Xie and Xiao* [2014].

Acknowledgments

The source code of DSHARK is made available over the open source version control system GitHub (see: https://github.com/pastfalk/DSHARK). The presented results are available from the corresponding author (patrick.astfalk@ipp.mpg.de). The research leading to the presented results has received funding from the European Research Council under the European Unions Seventh Framework Programme (FP7/2007-2013)/ERC grant agreement 277870. This work was facilitated by the Max-Planck/Princeton Center for Plasma Physics. The authors warmly acknowledge F. Califano for fruitful discussions and for providing the HVM code. We also thank T. Ooura for providing his numerical integration algorithm DE quadrature. All numerical results were obtained on the HPC cluster Hydra of the Rechenzentrum Garching (RZG), Germany. Furthermore, we thank T. Hayward and the referees for helpful comments and suggestions for modifications.

Michael Balikhin thanks K. Stasiewicz and another reviewer for their assistance in evaluating the paper.

References

Abraham-Shrauner, B., and W. C. Feldman (1977), Electromagnetic ion-cyclotron wave growth rates and their variation with velocity distribution function shape, *J. Plasma Phys.*, *17*, 123–131.

Achterberg, A., and C. A. Norman (1980), Particle acceleration by shock waves in solar flares, *Astron. Astrophys.*, *89*, 353–362.

Brambilla, M. (Ed.) (1998), *Kinetic Theory of Plasma Waves: Homogeneous Plasmas*, Oxford Univ. Press, New York.

Decker, R. B., S. M. Krimigis, E. C. Roelof, M. E. Hill, T. P. Armstrong, G. Gloeckler, D. C. Hamilton, and L. J. Lanzerotti (2005), Voyager 1 in the foreshock, termination shock, and heliosheath, *Science*, *309*, 2020–2024, doi:10.1126/science.1117569.

Fisk, L. A., and G. Gloeckler (2006), The common spectrum for accelerated ions in the quiet-time solar wind, *Astrophys. J.*, *640*, L79–L82, doi:10.1086/503293.

Fried, B. D., and S. D. Conte (1961), *The Plasma Dispersion Function*, Academic Press, New York.

Gaelzer, R., and L. F. Ziebell (2014), The dispersion relations of dispersive Alfvén waves in superthermal plasmas, *J. Geophys. Res. Space Physics*, *119*, 9334–9356, doi:10.1002/2014JA020667.

Gerald, C. F., and P. O. Wheatley (2003), *Applied Numerical Analysis*, Pearson, New York.

Gloeckler, G., et al. (1992), The solar wind ion composition spectrometer, *Astron. Astrophys. Suppl. Ser.*, *92*, 267–289.

Hasegawa, A., K. Mima, and M. Duong-van (1985), Plasma distribution function in a superthermal radiation field, *Phys. Rev. Lett.*, *54*, 2608–2610, doi:10.1103/PhysRevLett.54.2608.

Hellinger, P., and H. Matsumoto (2000), New kinetic instability: Oblique Alfvén fire hose, *J. Geophys. Res.*, *105*, 10,519–10,526, doi:10.1029/1999JA000297.

Jones, F. C., and D. C. Ellison (1991), The plasma physics of shock acceleration, *Space Sci. Rev.*, *58*, 259–346, doi:10.1007/BF01206003.

Ko, Y.-K., L. A. Fisk, G. Gloeckler, and J. Geiss (1996), Limitations on suprathermal tails of electrons in the lower solar corona, *Geophys. Res. Lett.*, *23*, 2785–2788, doi:10.1029/96GL02449.

Krimigis, S. M., J. F. Carbary, E. P. Keath, T. P. Armstrong, L. J. Lanzerotti, and G. Gloeckler (1983), General characteristics of hot plasma and energetic particles in the Saturnian magnetosphere—Results from the Voyager spacecraft, *J. Geophys. Res.*, *88*, 8871–8892, doi:10.1029/JA088iA11p08871.

Lazar, M., and S. Poedts (2014), Instability of the parallel electromagnetic modes in Kappa distributed plasmas—II. Electromagnetic ion-cyclotron modes, *Mon. Not. R. Astron. Soc.*, *437*, 641–648, doi:10.1093/mnras/stt1914.

Lazar, M., S. Poedts, and R. Schlickeiser (2011), Proton firehose instability in bi-Kappa distributed plasmas, *Astron. Astrophys.*, *534*, A116, doi:10.1051/0004-6361/201116982.

Leubner, M. P. (1982), On Jupiter's whistler emission, *J. Geophys. Res.*, *87*, 6335–6338, doi:10.1029/JA087iA08p06335.

Leubner, M. P. (2000), Wave induced suprathermal tail generation of electron velocity space distributions, *Planet. Space Sci.*, *48*, 133–141, doi:10.1016/S0032-0633(99)00091-4.

Leubner, M. P. (2002), A nonextensive entropy approach to kappa-distributions, *Astrophys. Space Sci.*, *282*, 573–579, doi:10.1023/A:1020990413487.

Leubner, M. P., and N. Schupfer (2000), Mirror instability thresholds in suprathermal space plasmas, *J. Geophys. Res.*, *105*, 27,387–27,392, doi:10.1029/1999JA000447.

Mace, R. L., and M. A. Hellberg (1995), A dispersion function for plasmas containing superthermal particles, *Phys. Plasmas*, *2*, 2098–2109, doi:10.1063/1.871296.

Maksimovic, M., V. Pierrard, and P. Riley (1997), Ulysses electron distributions fitted with Kappa functions, *Geophys. Res. Lett.*, *24*, 1151–1154, doi:10.1029/97GL00992.

Mangeney, A., F. Califano, C. Cavazzoni, and P. Travnicek (2002), A numerical scheme for the integration of the Vlasov-Maxwell system of equations, *J. Comput. Phys.*, *179*, 495–538, doi:10.1006/jcph.2002.7071.

Martin, P., and M. A. Gonzalez (1979), New two-pole approximation for the plasma dispersion function Z, *Phys. Fluids*, *22*, 1413, doi:10.1063/1.862727.

Meyer-Vernet, N., M. Moncuquet, and S. Hoang (1995), Temperature inversion in the Io plasma torus, *Icarus*, *116*, 202–213, doi:10.1006/icar.1995.1121.

Miller, J. A. (1991), Magnetohydrodynamic turbulence dissipation and stochastic proton acceleration in solar flares, *Astrophys. J.*, *376*, 342–354, doi:10.1086/170284.

Olbert, S. (1968), Summary of experimental results from M.I.T. detector on IMP-1, in *Physics of the Magnetosphere, Astrophys. and Space Sci. Lib.*, vol. 10, edited by R. D. L. Carovillano, J. F. McClay, and H. R. Radoski, pp. 641–659, Springer, Netherlands.

Paschalidis, N. P., E. T. Sarris, S. M. Krimigis, R. W. McEntire, M. D. Levine, I. A. Daglis, and G. C. Anagnostopoulos (1994), Energetic ion distributions on both sides of the Earth's magnetopause, *J. Geophys. Res.*, *99*, 8687–8703, doi:10.1029/93JA03563.

Pavlos, G. P., L. P. Karakatsanis, M. N. Xenakis, A. E. G. Pavlos, A. C. Iliopoulos, and D. V. Sarafopoulos (2012), Tsallis non-extensive statistics. Theory and applications. ArXiv e-prints.

Roennmark, K. (1982), Waves in homogeneous, anisotropic multicomponent plasmas (WHAMP), *Tech. Rep.*, Kiruna Geophys. Inst., Kiruna, Sweden.

Silva, R., A. R. Plastino, and J. A. S. Lima (2002), A Maxwellian path to the q-nonextensive velocity distribution function, eprint arXiv:cond-mat/0201503.

Summers, D., and R. M. Thorne (1991), The modified plasma dispersion function, *Phys. Fluids B*, *3*, 1835–1847, doi:10.1063/1.859653.

Summers, D., S. Xue, and R. M. Thorne (1994), Calculation of the dielectric tensor for a generalized Lorentzian (kappa) distribution function, *Phys. Plasmas*, *1*, 2012–2025, doi:10.1063/1.870656.

Takahasi, H., and M. Mori (1974), Double exponential formulas for numerical integration, *Res. Inst. Math. Sci. Lib., Kyoto Univ.*, *9*, 721–741.

Treumann, R. A. (1999), Kinetic theoretical foundation of Lorentzian statistical mechanics, *Phys. Scr.*, *59*, 19–26, doi:10.1238/Physica.Regular.059a00019.

Tsallis, C. (1988), Possible generalization of Boltzmann-Gibbs statistics, *J. Stat. Phys.*, *52*(1–2), 479–487.

Valentini, F., P. Trávníček, F. Califano, P. Hellinger, and A. Mangeney (2007), A hybrid-Vlasov model based on the current advance method for the simulation of collisionless magnetized plasma, *J. Comput. Phys.*, *225*, 753–770, doi:10.1016/j.jcp.2007.01.001.

Vasyliunas, V. M. (1968), A survey of low-energy electrons in the evening sector of the magnetosphere with OGO 1 and OGO 3, *J. Geophys. Res.*, *73*, 2839–2884, doi:10.1029/JA073i009p02839.

Xie, H.-s., and Y. Xiao (2014), PDRK: A general kinetic dispersion relation solver for magnetized plasma. ArXiv e-prints.

Xue, S., R. M. Thorne, and D. Summers (1996), Growth and damping of oblique electromagnetic ion cyclotron waves in the Earth's magnetosphere, *J. Geophys. Res.*, *101*, 15,457–15,466, doi:10.1029/96JA01088.

Yoon, P. H. (2012), Asymptotic equilibrium between Langmuir turbulence and suprathermal electrons in three dimensions, *Phys. Plasmas*, *19*(1), 012304, doi:10.1063/1.3676159.